超薄氧化層 n-MOSFET 元件之低頻雜訊分析

學生：游建文　　　　　　　　指導教授：汪大暉博士

國立交通大學　電子工程學系　電子研究所

摘要

本文探討了閘極氧化層厚度在直接穿遂範圍的 n-MOSFET 之低頻 1/f 雜訊。對 14Å 氧化層厚度而言，我們觀察到額外增加的低頻雜訊是電子和電洞藉由介面的缺陷結合所導致的。在如此薄的氧化層，價電層電子會發生穿遂而導致電子和電洞的費米能階分裂。這額外的低頻雜訊被歸因於電子和電洞佔據準費米能階之間的介面缺陷。

本文也探討了有著浮動體極的超薄氧化層 n-MOSFET 上，軟性崩潰位置對於低頻 1/f 雜訊會有所衝擊。在通道崩潰的元件，過量的雜訊現象可以在歐姆操作區域內被看到。這額外雜訊密度的量比較背景的 1/f 雜訊可大上十倍。這雜訊的來源被相信是和因軟性崩潰而加強電子穿遂價電帶所導致的浮動體極效應有關。作者指出，通道的軟性崩潰會增加汲極電流的雜訊，在部分空乏的類比 SOI 電路上，會是一個可靠度的問題。

Analysis of Flicker Noise Mechanism in Ultra-Thin Oxide n-MOSFETs

Student: Jian-Wen You Advisor: Dr. Tahui Wang

Department of Electronics Engineering & Institute of Electronics

National Chiao Tung University

Hsinch, Taiwan, R.O.C

Abstract

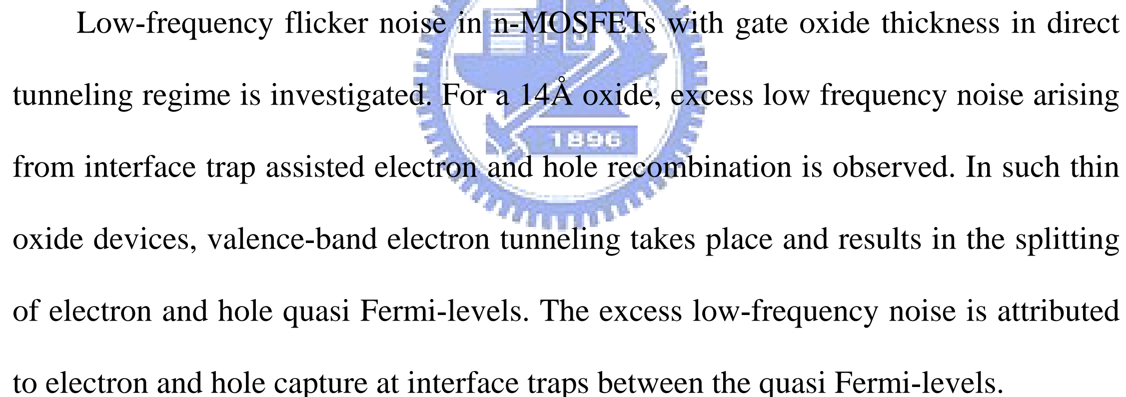

Low-frequency flicker noise in n-MOSFETs with gate oxide thickness in direct tunneling regime is investigated. For a 14Å oxide, excess low frequency noise arising from interface trap assisted electron and hole recombination is observed. In such thin oxide devices, valence-band electron tunneling takes place and results in the splitting of electron and hole quasi Fermi-levels. The excess low-frequency noise is attributed to electron and hole capture at interface traps between the quasi Fermi-levels.

The impact of soft breakdown location on low-frequency noise in ultra-thin oxide n-MOSFETs with floating body is also investigated. In a channel breakdown device, a noise overshoot phenomenon is observed in the ohmic regime. This excess noise spectral density is about one order of magnitude higher than the background 1/f noise. The origin of this excess noise is believed due to soft breakdown (SBD) enhanced valance-band electron tunneling and thus induced floating body effect. Our findings indicate that channel SBD enhanced drain current noise degradation can be a reliability issue in partially depleted analog SOI CMOS circuit.

Acknowledgement

I would like to express my sincere gratitude to my advisor, Dr. Tahui Wang for his support and guidance on my research. He was kind to discuss with me and correct my mistakes. Without his help, I would not finish this thesis smoothly. I also would like to offer my thanks to J.W. Wu and M.C. Chen, who assist me in many problems I met in the research. Then, I acknowledge my up-classmate, S.H. Ku, C.T. Chan, for their valuable technical and experimental supports as a great help for me. In addition, I would like to thank down-classmate, Huan-Chi Ma, for considerable helpful discussions and experiment supports. Besides, C.T. Chan and M.T. Wang are much appreciated for their very kind support in friendship.

I would like to appreciate my parent. They gave me much devotion and inspiration under my frustration without asking for paying-back. I thank all my lovely friends.

Contents

Chinese Abstract i

English Abstract ii

Acknowledgements iii

Contents iv

Figure Captions vi

Chapter1 Introduction 1

Chapter2 Fundamentals of Low-Frequency Noise in MOSFETs 3

2.1 Introduction 3

2.2 Unified Flicker Noise Model 3

2.3 Random Telegraph Noise Theory 4

2.4 Measurement of Noise Power Spectral Density and RTS 9

2.4.1 Noise Power Spectral Density Measurement 9

2.4.2 RTS Measurement 9

Chapter3 Observation of Excess Generation/Recombination Noise in Ultra-Thin Oxide (14Å) n-MOSFETs 13

3.1 Introduction 13

3.2 Observation of an Abnormal Increase of Flicker Noise 14

3.3 Analysis of RTS Noise Behavior 22

3.4 A New G-R Noise Mechanism 27

Chapter4 Excess Low-Frequency Noise in Floating Body Ultra-Thin Gate Oxide n-MOSFETs 33

4.1 Introduction 33

4.2 Excess Low-Frequency Noise Model in SOI MOSFETs 33

4.3 Kink Effect Induced Excess Low-Frequency Noise 36

4.4 Channel Soft Breakdown Enhanced Excess Low-Frequency Noise **43**

Chapter5 Conclusion **53**

References

Figure Captions

Fig. 2.1(a) Sample RTS in the drain current of a NMOS with W/L=0.32μm /0.12 μm. Vg=0.9V, Vd=0. 2V.

Fig. 2.1(b) The current interval between two max numbers of the drain current can be used to extract ΔI and the two peaks of the drain current shows clearly two-level RTS.

Fig. 2.2 Normalized current noise spectrum density for RTS with a Lorentzian fitting.

Fig. 2.3 A Low-frequency noise measurement setup.

Fig. 2.4 Block diagram of experimental setup used for the measurement of RTS in MOSFETs.

Fig. 2.5 The photograph of our micro-second measurement system.

Fig. 3.1 Normalized noise power spectral density (measured at Vd=0.2V, Vg-overdrive=0.7V, f=100Hz) versus gate oxide thickness in n-MOSFETs. There is an abnormal increase in noise level for the 14Å gate oxide device.

Fig. 3.2 Lorentzian power spectral density with the Vg-overdrive in a small n-MOSFET with 14 Å gate oxide.

Fig. 3.3(a) Normalized noise power spectral density versus Vg-overdrive at f=100Hz in small n-MOSFETs with **14** Å gate oxide.

Fig. 3.3(b) Normalized noise power spectral density versus Vg-overdrive at f=100Hz in small n-MOSFETs with **64** Å gate oxide.

Fig. 3.4(a) Temperature dependence for the Lorentzian noise in a small area n-MOSFET with an oxide thickness of 14Å.

Fig. 3.4(b) Temperature dependence for $((S_{id}/I_d^2)*f)$

Fig. 3.5 Arrhenius plot of trap time-constant versus 1000/T. The carrier capture time (τ) according to the Shockly-Read-Hall theory is also shown. The linear behavior of the Arrhenius plot reveals that the source of the noise is related to carrier capture/emission by an interface trap.

Fig. 3.6 Measured Lorentzian noise power spectral density of a small area n-MOSFET for two gate voltages (Vg=0.6V, 1.3V). The corner frequency (fc), which reflects the trap time constant (τ), changes to a lower value as the Vg increases.

Fig. 3.7 RTS in a small n-MOSFET (W/L=0.16 μm/0.12 μm) with 14 Å gate oxide is measured in the weak inversion region (Vg=0.65 V、0.7 V、0.8 V、0.9) at the time interval of 20(ms).

Fig. 3.8 RTS in a small n-MOSFET (W/L=0.16 μm/0.12 μm) with 14 Å gate oxide is measured in the strong inversion region (Vg=1.1 V、1.2 V、1.4 V、1.6 V) at the time interval of 5(s).

Fig. 3.9 Average t_L and t_H versus gate voltage in a small area (W/L=0.16μm/0.12μm) n-MOSFET in weak inversion.

Fig. 3.10 Average t_L and t_H versus gate voltage in a small area (W/L=0.16μm/0.12μm) n-MOSFET in strong inversion .

Fig. 3.11 The corresponding electron occupation factor (ft) versus Vg. When ft is equal to 0.5, gate voltages are equal to 0.7V and 1.5V, respectively.

Fig. 3.12 The corresponding normalized noise power spectral density versus Vg at f = 100 (Hz). The noise level has maximum values at Vg=0.7V and 1.5V.

Fig. 3.13(a) Substrate current versus gate bias with Vd=Vs=0V.

Fig. 3.13(b) Illustration of valence-band electron tunneling and electron and hole recombination at an interface trap.

Fig. 4.1(a) Shot noise sources in an SOI MOSFET operating in strong inversion.

Fig. 4.1(b) The noise small-signal equivalent circuit for the floating body.

Fig. 4.2 The I_d-V_d characteristics in NMOS devices with floating body and grounded body when gate is biased at 0.9V.

Fig. 4.3 Normalization noise power density in floating body NMOS at different drain voltage. Gate is biased at 0.9V.

Fig. 4.4 Normalization noise power spectral density in grounded body NMOS at different drain voltages. Gate is biased at 0.9V.

Fig. 4.5 Normalization noise power spectral density in floating body NMOS at different drain voltage. Gate is biased at 0.9V.

Fig. 4.6 Comparison of normalization noise power spectral density under different drain bias in floating body NMOS and grounded body NMOS for given frequency.

Table .1 The ratio of I_d/I_s+I_d and I_b/I_s+I_d before and after SBD in two n-MOSFETs are shown.

Fig. 4.7 The gate current and substrate current as a function of Vg in fresh, channel SBD, and edge SBD n-MOSFETs were compared.

Fig. 4.8(a) Valence band electron tunneling induced floating-body charging in a c-SBD n-MOSFET

Fig. 4.8(b) The drain-induced floating-body charging in an e-SBD n-MOSFET.

Fig. 4.9 The low frequency noise power spectrums of n-MOSFET before and after both SBD modes are shown .The measurement drain bias is 0.1V and the gate bias is 1.2V.

Fig. 4.10 The normalized noise power spectrum of a c-SBD n-MOSFETs with floating body under different gate biases is shown.

Fig. 4.11 Comparison of normalization noise power density under different gate bias in the flesh device, c-SBD device and e-SBD device at f=100(Hz).